Journal of Materials Science & Nanotechnology
Volume 9 | Issue 3
ISSN: 2348-9812

Research Article Open Access

Numerical Analysis on the Electromechanical Behaviors and Piezotronic Effects Controlled by the Applied of Initial Stress

Ben Salah I[*1,2], Takali F[1,3] and Njeh A[1]

[1]Laboratory of Physics of Materials, Faculty of Sciences of Sfax, University of Sfax, Sfax, Tunisia

[2]Sfax Preparatory Engineering Institute, Street Menzel Chaker Km, Sfax, Tunisia

[3]National School of Engineers of Sfax (ENIS), Street Soukra Km, Sfax, Tunisia

Corresponding author: Ben Salah I, Laboratory of Physics of Materials, Faculty of Sciences of Sfax, University of Sfax, BP 815, 3018 Sfax, Tunisia, Tel: +21655560779, E-mail: bs_issam@yahoo.fr

Received Date: October 22, 2021 **Accepted Date:** November 29, 2021 **Published Date:** December 01, 2021

Citation: Ben Salah I, Takali F, Njeh A (2021) Numerical Analysis on the Electromechanical Behaviors and Piezotronic Effects Controlled by the Applied of Initial Stress. J Mater Sci Nanotechnol 9(3): 302

Abstract

Based on the linear three-dimensional elastic theory, shear horizontal (SH) wave propagation along the normal direction to the piezoelectric semiconductor plate (PSC) was obtained in the presence of initial horizontal and vertical stresses. The purpose behind obtaining the numerical solutions was to evaluate the effect of stress on dimensionless frequency and phase velocity. To verify the exactness of the process, the dispersion curves of phase velocity in a piezoelectric semiconductor plate without loaded initial stresses were calculated beforehand by the proposed approach to compare with those reported in the literature. Next, a series of cases of initial stress were further executed to explore the effects of horizontal initial stress and vertical initial stress on the SH0 and SH1 wave modes. The results revealed that the positive initial tensile stress led to the increase in the phase velocity, while the preliminary negative compressive stress decreased the phase velocity. Finally, the effect of the initial stress on the electromechanical fields was explained in detail. The obtained results offer a predictable and theoretical fundament for the development of piezoelectric semiconductor structures under the influence of initial stress to acoustic wave devices.

Keywords: Piezoelectric Semiconductor; Shear Horizontal Waves; Initial Stress; Dispersion Curves; Phase Velocity; Electromechanical Fields

Introduction

Piezoelectric (PS) materials can be recognized as dielectrics or semiconductors. In PS semiconductors (PS conductors), since the induced electric field produces electric current, these smart materials possess piezoelectric effect and semiconductor properties [1,2]. Due to their prevalent physical properties, PSCs have been broadly used in surface acoustic wave devices, electronic sensors, and energy harvesting [3]. At the same time, a great deal of research has been realized on the physical properties of PSCs, such as acoustoelectric, photoelectric, photothermal and piezoelectric effects [4-6]. Moreover, novel piezoelectric semiconductor nanostructures, such as ZnO fibers, tubes, belts, spirals and films have been synthesized [7-10]. In this regard zinc oxide (ZnO) is in fact one of the most important multi-functional semiconductors, which has drawn much attention thanks to its many unique properties as low toxicity, high fluorescence activity and relatively strong piezoelectric effect [11]. This makes it an interesting electromechanical coupling material for various piezoelectric applications [12]. Numerous kinds of one-dimensional (1D) ZnO nanostructures, such as nanowires, nanorods, nanotubes, nano-belts, etc. have attracted much interest as building blocks for various fascinating nanodevices applications such as electronics, optics, and nano-electromechanical systems (NEMS) [13]. In recent years, diverse applications based on piezoelectric properties of ZnO nanostructures grown on a variety of conventional substrates, namely piezoelectric field effect transistors, the piezoelectric diode, piezoelectric sensors and the piezoelectric nano-generator, [14-16] have been demonstrated.

For device applications, the basic behaviors of piezoelectric semiconductors can be described by a phenomenological theory consisting of the equations of linear piezoelectricity [17] and the conservation of charge for electrons and holes [18]. The theory has been used in a series of useful applications of PSC, including thickness vibration of plates [19], propagation of plate and surface waves [10,20,21], electromechanical fields in an inclusion [22], fields near cracks [23,24], static extension of a fiber [25], bending of a fiber [26], and static fields near stress-free PN junctions [27].

A PS material may also demonstrate an initial stress effect, i.e., an initial stress in the multi-layered structures can lead to delamination, microcracking, debonding and degradation of the layer. It can also lead to the dramatic change of dispersion relation corresponding to the wave propagation in the above-mentioned structures. Meanwhile, the effects of initial stresses on bulk wave propagation in layered piezomagnetic/piezoelectric plates, with a special focus on the phase velocities and frequency spectrum have been investigated in [28]. Furthermore, the effects of initial stress on the propagation behavior and dispersion relation of shear horizontal (SH) waves in piezoelectric plates have been studied numerically [29-32]. Concerning the study of the effects of initial stress on the reflection and transmission of waves at the interface between two piezoelectric half spaces, it has been carried out in [33]. The influence of compressive and tensile initial stresses on the behaviors of Lamb and SH waves in a prestressed multilayered PZT-4/PZT-5A composites system has also been considered [34]. Moreover, the effects of initial stress on the electromechanical coupling factor of SH wave in layered piezoelectric structures have been investigated as well [35]. The performance of $Sc_{43\%}$ $AlN_{57\%}$/ZnO/diamond piezoelectric hetero-structures using matrix and polynomial methods under uniaxial stress have been developed [36]. In the same context, Shams [37] has demonstrated the effects of initial stress on the phase velocities of surface Love wave in hetero-structures, while Sahu et al. [38] has explored a similar problem in the piezo-composite structure composed of functionally graded piezoelectric material (FGPM).

Considering all these facts, it is also necessary that the effects of initial stresses be analyzed exhaustively as has been realized in a piezoelectric semiconductor (PSC) fiber under local extensional or compressive stress [39] and under axial force [6-16]. Unlike most of the existing literature in which only the effects of normal initial stress have been examined, in the present research work, the authors have explored the effects of two types of initial stresses, namely normal and shear initial stresses on the propagation behavior of shear waves (SH-waves) in a piezoelectric semiconductor plate.

Part of the recent studies on piezoelectric semiconductors has formed a new area of research called piezotronics and piezophototronics [40,41]. In piezotronic devices, the motion of charge carriers is manipulated by mechanical charges through the accompanying electric field via piezoelectric coupling. For piezotronic applications, the effects of end forces on moving loads in the bending and

extension of piezoelectric semiconductor fibers have been investigated [42,43]. The study of stress effects on PN junctions and metal-semiconductor junctions has also been caried out [44]. It should be mentioned that in the relatively recent literature, some researchers have used the above theory of piezoelectric semiconductors to study the propagation of elastic waves in piezoelectric semiconductors [10,14,30-32].

To the authors' best knowledge, however, no work on wave propagation in piezoelectric semiconductor plate under an initial stress has been reported, which motivates the present study. This paper focusses on the propagation characteristic of SH waves in the PSC plate under an initial horizontal and vertical stress.

This paper is organized as follows. In sections 2 and 3, the problem to be solved via the phenomenological theory of piezoelectric semiconductor materials is described. It consists of the equation of motion, the charge equation of electrostatics, and the conservation of charge for electrons and holes. In section 4, the dispersion equation in PSC plate under an initial stress is derived based on numerical resolution by a system to the eigenvalues and eigenvectors and the interface and boundary conditions. In section 5, the effect of initial horizontal and vertical stress on the dispersion curves of SH wave in a PSC plate are presented in detail. The effect of initial stress on the electromechanical fields of PSC plate are investigated in Section 5.4. Finally, conclusions are drawn in Section 6.

Phenomenological theory of piezoelectric semiconductors

In this section, a brief summary of the general 3D equations for piezoelectric semiconductors with initial stresses are presented. From the basic behavior of PSC is described by a phenomenological, coupled-field theory consisting of the equations of linear piezoelectricity [10] and the conservation of charge for holes and electrons. The Cartesian tensor notation is employed in this paper. Indices i,j,k and l assume 1, 2, and 3. A comma followed by an index indicates partial differentiation with respect to the coordinate associated with the index. A superimposed dot "." represents a time derivative. The theory consists of [10]:

$$T_{ij,j} = \rho \ddot{u}_i, \quad (1a)$$

$$D_{i,i} = q(p - n + N_D^+ - N_A^-), \quad (1b)$$

$$J_{i,i}^p = -q\dot{p}, \quad (1c)$$

$$J_{i,i}^n = q\dot{n}, \quad (1d)$$

where T_{ij}, u_i and D_i are the components of stresses, mechanical and electric displacements, respectively. ρ is the mass density, q is the electronic charge with 1.6×10^{-19} Coulomb, p and n the concentrations of holes and electrons, N_D^+ and N_A^- are the concentrations of impurities of donors and acceptors, respectively. Finally, J_i^p and J_i^n are the hole and electron current densities, respectively.

(1a) is the stress equation of motion or the linear momentum equation (Newton's law). (1b) is the charge equation of electrostatics (Gauss's law). (1c) and (1d) are the conservation of charge for holes and electrons, respectively, which are also called continuity equations. Constitutive relations accompanying (1a), (1b), (1c) and (1d) can be written in the following form [6,10]:

$$T_{ij} = c_{ijkl} S_{kl} - e_{kij} E_k, \quad (2a)$$

$$D_i = e_{ikl} S_{kl} + \varepsilon_{ik} E_k, \quad (2b)$$

$$J_i^p = qp\mu_{ij}^p E_j - qD_{ij}^p p_{,j}, \quad (2c)$$

$$J_i^n = qn\mu_{ij}^n E_j + qD_{ij}^n n_{,j}, \quad (2d)$$

In which S_{kl} and E_k represent the strain and electric field, respectively. c_{ijkl}, e_{kij} and ε_{ik} are elastic, piezoelectric and dielectric constants, respectively. Moreover, μ_{ij}^n and μ_{ij}^p, D_{ij}^n and D_{ij}^p are the carrier mobility and the carrier diffusion constants, respectively, and the indices n and p correspond to the two cases of holes and electrons, respectively. (2a) and (2b) are the usual constitutive relations for piezoelectric materials. (2c) and (2d) are for hole and electron currents including both drift currents under an electric field and diffusion currents due to concentration gradients, respectively. The strain and the electric field are related to the mechanical displacement u_i and the electric potential ϕ through.

$$S_{ij} = (u_{i,j} + u_{j,i})/2, \quad (3a)$$

$$E_i = -\phi_{,i}, \quad (3b)$$

By considering the disturbance of the carriers, the concentrations of holes and electrons can be written as

$$p = p_0 + \Delta p, n = n_0 + \Delta n, \quad (4)$$

in which p_0 and n_0 are the initial concentrations of carriers, Δp and Δn are the variation of the electron and hole concentration, respectively. If uniform impurities are considered, we can obtain

$$p_0 = N_A^-, n_0 = N_D^+ \quad (5)$$

In (4), Δp and Δn are perturbations of holes and electrons, respectively. Then (2b, c and d) takes the following form

$$D_{i,i} = q(\Delta p - \Delta n) \quad (6a)$$

$$q\frac{\partial}{\partial t}(\Delta p) = -J_{i,i}^p, \quad (6b)$$

$$q\frac{\partial}{\partial t}(\Delta n) = J_{i,i}^n, \quad (6c)$$

For the case of small perturbations of Δp and Δn, the hole and electron currents in (2c and 2d) can be linearized as

$$J_i^p = qp\mu_{ij}^p E_j - qD_{ij}^p(\Delta p)_{,j}, \quad (7a)$$

$$J_i^n = qn\mu_{ij}^n E_j + qD_{ij}^n(\Delta n)_{,j}, \quad (7b)$$

Anti-plane problems for the crystals of 6mm symmetry

The crystals of 6mm symmetry include widely used materials like Zinc Oxide (ZnO) [10]. For this crystal, the material tensors in Eqs. (2a, b, c and d) can be represented by the following matrices under the compact matrix notation

$$[c_{\alpha\beta}] = \begin{pmatrix} c_{11} & c_{12} & c_{13} & 0 & 0 & 0 \\ c_{21} & c_{22} & c_{23} & 0 & 0 & 0 \\ c_{31} & c_{32} & c_{33} & 0 & 0 & 0 \\ 0 & 0 & 0 & c_{44} & 0 & 0 \\ 0 & 0 & 0 & 0 & c_{55} & 0 \\ 0 & 0 & 0 & 0 & 0 & c_{66} \end{pmatrix}, [e_{i\alpha}] = \begin{pmatrix} 0 & 0 & e_{31} \\ 0 & 0 & e_{31} \\ 0 & 0 & e_{33} \\ 0 & e_{15} & 0 \\ e_{15} & 0 & 0 \\ 0 & 0 & 0 \end{pmatrix}^T, [\varepsilon_{ij}] = \begin{pmatrix} \varepsilon_{11} & 0 & 0 \\ 0 & \varepsilon_{22} & 0 \\ 0 & 0 & \varepsilon_{33} \end{pmatrix} (8)$$

where $c_{66} = (c_{11} - c_{12})/2$, and the superscript T is for matrix transpose. μ_{ij} and D_{ij} have the same structure as ε_{ij}.We consider motions with $\partial/\partial x_3 = 0$. Then Eq. (4) splits into a plane strain problem for u_1 and u_2, and an anti-plane problem for

$$u_3 = u(x_1, x_2, t), \phi = \phi(x_1, x_2, t),$$

$$\Delta p = \Delta p(x_1, x_2, t), \Delta n = \Delta n(x_1, x_2, t). (9)$$

For the anti-plane problem, the strain and electric field components are

$$\begin{Bmatrix} 2S_{31} \\ 2S_{32} \end{Bmatrix} = \nabla u_3, \begin{Bmatrix} E_1 \\ E_2 \end{Bmatrix} = -\nabla \phi (10)$$

where $\nabla = i_1\partial_1 + i_2\partial_2$ is the two-dimensional gradient operator. The nontrivial components of T_{ij}, D_i, J_i^p and J_i^n are

$$\begin{Bmatrix} T_{31} \\ T_{32} \end{Bmatrix} = c_{44}\nabla u_3 + e_{15}\nabla \phi, (11)$$

$$\begin{Bmatrix} D_1 \\ D_2 \end{Bmatrix} = e_{15}\nabla u_3 - \varepsilon_{11}\nabla \phi, (12)$$

$$\begin{Bmatrix} J_1^p \\ J_2^p \end{Bmatrix} = -qp_0\mu_{11}^p\nabla \phi - qD_{11}^p\nabla(\Delta p), \begin{Bmatrix} J_1^n \\ J_2^n \end{Bmatrix} = -qn_0\mu_{11}^n\nabla \phi + qD_{11}^n\nabla(\Delta n) (13)$$

The nontrivial ones of the equations of motion and charge Eqs. (1a and b) take the following form:

$$c_{44}\nabla^2 u_3 + e_{15}\nabla^2\phi = \rho \ddot{u}_3$$

$$e_{15}\nabla^2 u_3 - \varepsilon_{11}\nabla^2\phi = q(\Delta p - \Delta n), (14)$$

And for the Eqs. (1c and d) can be written

$$\frac{\partial}{\partial t}(\Delta p) = p_0\mu_{11}^p\nabla^2\phi - D_{11}^p\nabla^2(\Delta p),$$

$$\frac{\partial}{\partial t}(\Delta n) = -n_0\mu_{11}^n\nabla^2\phi + D_{11}^n\nabla^2(\Delta n), (15)$$

where ∇^2 is the two-dimensional Laplacian $\nabla^2 = \partial^2/\partial x_1^2 + \partial^2/\partial x_2^2$

Shear-horizontal waves

As shown in Figure 1, a piezoelectric semiconductor plate is taken into account. It involves a PSC plate with the thickness of $h = 1\ \mu m$ with the total thickness of $2\ \mu m$. We take the origin of cartesian coordinate system $ox_1x_2x_3$ at any point on the mid-plane of the semiconductor layer and x_2-axis along the thickness of the layer as shown in Figure 1 The piezoelectric semiconductor plate is polarized along the x_3-axis direction, perpendicular to the x_1-x_2 plane. It is assumed that there exists constant initial horizontal and vertical stress (Tensile and compression) in the piezoelectric semiconductor plate.

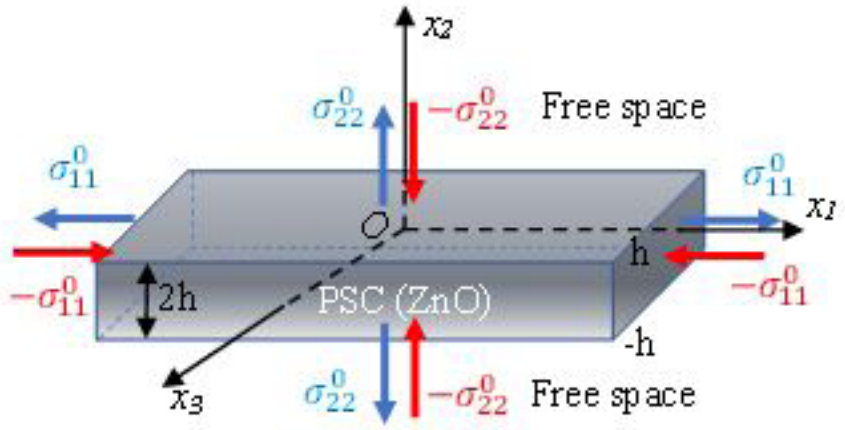

Figure 1: Schematic diagram of coordinate systems for piezoelectric semiconductor plate subjected to initial stress

The harmonic solutions to (14-15) are considered when the waves propagating in the x_1 direction, and they have the following forms

$$\begin{Bmatrix} u_3 \\ \phi \\ \Delta p \\ \Delta n \end{Bmatrix} = \begin{Bmatrix} A \\ B \\ C \\ D \end{Bmatrix} exp(\lambda x_2)\, exp[i(k x_1 - \omega t)] \quad (16)$$

where A, B, C, and D are constants. ω is real and positive. The real part of k is positive. Substituting (16) into (14) and (15) results in four linear homogeneous algebraic equations for A, B, C and D. Then, combining Eqs. (14) and (15) to (16), the following linear eigenvalue system is obtained:

$$[K_{ij}]\begin{bmatrix} a \\ b \end{bmatrix} = \lambda \begin{bmatrix} a \\ b \end{bmatrix} \quad (17)$$

where $a=[u_3\ \phi\ \Delta p\ \Delta n]^T$ is related to the generalized displacement vector, $b=[T_{23}\ D_2\ J^p\ J^n]^T$ to the generalized traction vector, where superscript T denotes the vector transpose. The matrices $[K_{ij}]$ are defined as

$$[K_{ij}] = \begin{bmatrix} 0 & 0 & 0 & 0 & K_{15} & K_{16} & 0 & 0 \\ 0 & 0 & 0 & 0 & K_{25} & K_{26} & 0 & 0 \\ 0 & 0 & 0 & 0 & K_{35} & K_{36} & K_{37} & 0 \\ 0 & 0 & 0 & 0 & K_{45} & K_{46} & 0 & K_{48} \\ K_{51} & K_{52} & 0 & 0 & 0 & 0 & 0 & 0 \\ 0 & K_{62} & K_{63} & K_{64} & 0 & 0 & 0 & 0 \\ 0 & K_{72} & K_{73} & 0 & 0 & 0 & 0 & 0 \\ 0 & K_{82} & 0 & K_{84} & 0 & 0 & 0 & 0 \end{bmatrix} \quad (18)$$

The explicit expressions of elements in the matrix $[K_{ij}]$ are given in **Appendix A**. Eq. (18) is an eigenvalue/eigenvector system for the given wave number k and frequency ω. Solving Eq. (18) gives eight complex eigenvalues λ and their corresponding eigenvectors (***a***, ***b***) in PSC plate. The eight eigenvalues are divided into two groups as λ^+ and λ^- (also for the corresponding eigenvectors) such that λ^+ and λ^- have positive and negative imaginary parts, respectively. All eigenvalues are classified into two categories: If $Re(\lambda_i) > 0$ or $Re(\lambda_i) < 0$ and $Im(\lambda_i) > 0$ or $Im(\lambda_i) < 0$, denoting the real and imaginary parts of eigenvalues, respectively, where $i \in [1, \cdots, 8]$. In order to study the wave propagation in the PSC plate, we need the proper boundary conditions on the plate surfaces as considered below.

Boundary Conditions

Consider the plate is unelectroded. In the top and bottom free space of the plate, the electrical potential should satisfy [10,47]

$$\nabla^2\phi = 0, |x_2| > h,$$
$$\phi = 0,\ x_2 \to \pm\infty \quad (19)$$

The free space electric displacement is given by

$$D_i = -\varepsilon_0\phi_{,i} \quad (20)$$

According to Eq. (19), the harmonic solutions for electrical potential ϕ have the following forms

$$\phi = \begin{cases} G\ exp\,[k(h - x_2)]exp[i(k x_1 - \omega\, t)], x_2 > h, \\ H\ exp\,[k(h + x_2)]exp[i(k x_1 - \omega\, t)], x_2 < h, \end{cases} \quad (21)$$

where G and H are the amplitudes. It is noted that the real part of k must be positive so that the second relation in (19) can be satisfied. Substitute (21) into the equation (20), and then it can be obtained that

$$D_2 - \varepsilon_0 k\phi = 0, x_2 > h,$$
$$D_2 + \varepsilon_0 k\phi = 0, x_2 < -h, \quad (22)$$

At the top and bottom of the composite plate where $x_2 = \pm h$, there are six boundary and four continuity conditions:

$$T_{23}(\pm h) = 0, J_2^p(\pm h) = 0, J_2^n(\pm h) = 0,$$

$$\phi(h^+) = \phi(h^-), D_2(h^+) = D_2(h^-),$$

$$\phi(-h^+) = \phi(-h^-), D_2(-h^+) = D_2(-h^-), \quad (23)$$

Wave fields in the PSC plate

For nontrivial solutions, the determinant of the coefficient matrix of the equations has to vanish, which leads to a polynomial equation of degree eight for λ. The eight roots of this equation as $\lambda^{(m)}(k, \omega)$ and the corresponding nontrivial solution of A, B, C and D as $A^{(m)}$, $B^{(m)}$, $C^{(m)}$ and $D^{(m)}$ should be represented. It is to be noted that only the ratios among $A^{(m)}$, $B^{(m)}$, $C^{(m)}$ and $D^{(m)}$ can be determined. Then, the general solution of (14) and (15) can be written as

$$\begin{Bmatrix} u_3 \\ \phi \\ \Delta p \\ \Delta n \end{Bmatrix} = \sum_{m=1}^{8} F^{(m)} \begin{Bmatrix} A^{(m)} \\ B^{(m)} \\ C^{(m)} \\ D^{(m)} \end{Bmatrix} exp\left(\lambda^{(m)} x_2\right)\ exp[i(k x_1 - \omega\, t)] \quad (24)$$

where $F^{(m)}$ are undetermined constants.

Substituting Eqs. (24), (21) and (22) into Eq. (23), we obtain ten linear algebraic equations for $F^{(m)}$, G and H.
At $x_2 = \pm h$, the resulting equations will be:

$$\sum_{m=1}^{8} F^{(m)}\lambda^{(m)}exp\left(\lambda^{(m)}h\right)\left(c_{44}A^{(m)}+e_{15}B^{(m)}\right)=0$$

$$\sum_{m=1}^{8} F^{(m)}\lambda^{(m)}exp\left(-\lambda^{(m)}h\right)\left(c_{44}A^{(m)}+e_{15}B^{(m)}\right)=0$$

$$\sum_{m=1}^{8} F^{(m)}\lambda^{(m)}exp\left(\lambda^{(m)}h\right)\left(B^{(m)}\right)=G$$

$$\sum_{m=1}^{8} F^{(m)}\lambda^{(m)}exp\left(-\lambda^{(m)}h\right)\left(B^{(m)}\right)=H$$

$$\sum_{m=1}^{8} F^{(m)}\lambda^{(m)}exp\left(\lambda^{(m)}x_2\right)\left(e_{15}A^{(m)}-\varepsilon_{11}B^{(m)}\right)=\varepsilon_0 kG$$

$$\sum_{m=1}^{8} F^{(m)}\lambda^{(m)}exp\left(-\lambda^{(m)}h\right)\left(e_{15}A^{(m)}-\varepsilon_{11}B^{(m)}\right)=-\varepsilon_0 kH$$

$$\sum_{m=1}^{8} F^{(m)}\lambda^{(m)}exp\left(\lambda^{(m)}h\right)\left(-qp_0\mu^p B^{(m)}-qD^p C^{(m)}\right)=0$$

$$\sum_{m=1}^{8} F^{(m)}\lambda^{(m)}exp\left(-\lambda^{(m)}h\right)\left(-qp_0\mu^p B^{(m)}-qD^p C^{(m)}\right)=0$$

$$\sum_{m=1}^{8} F^{(m)}\lambda^{(m)}exp\left(\lambda^{(m)}h\right)\left(-qn_0\mu^n B^{(m)}+qD^n D^{(m)}\right)=0$$

$$\sum_{m=1}^{8} F^{(m)}\lambda^{(m)}exp\left(-\lambda^{(m)}h\right)\left(-qn_0\mu^n B^{(m)}+qD^n D^{(m)}\right)=0 \quad (25)$$

In Eq. (25), we obtain a system of homogeneous linear equation for the involved coefficient vectors $F^{(m)}$, G and H

$$\left[M_{ij}\right]\begin{bmatrix}F^{(m)}\\G\\H\end{bmatrix}=0, i,j=1,\cdots,10 \quad (26)$$

where $[M_{ij}]$ is a matrix 10 ×10, whose elements are given in **Appendix B**. The dispersion relation of the problem can be found by equating the determinant of matrix $[M_{ij}]$ to zero, which gives an equation that determines the dispersion relations of ω versus k, for which numerical solutions are presented in the section that follows.

Solution of the semiconductor plate with initial stress

The constitutive equations of the piezoelectric semiconductor plate Eq. (1a) under an initial stress σ_{kj}^0 can be written an developed as [29–33]

$$\rho\ddot{u}_i=T_{ij,j}+\left(u_{i,k}\sigma_{kj}^0\right)_{,j}$$

$$\rho\frac{\partial^2 u}{\partial t^2}=\frac{\partial}{\partial x_1}\left[T_{31}+\sigma_{11}^0\frac{\partial u}{\partial x_1}+\sigma_{12}^0\frac{\partial u}{\partial x_2}\right]+\frac{\partial}{\partial x_2}\left[T_{32}+\sigma_{21}^0\frac{\partial u}{\partial x_1}+\sigma_{22}^0\frac{\partial u}{\partial x_2}\right]$$

$$\rho\frac{\partial^2 u}{\partial t^2}=\frac{\partial T_{31}}{\partial x_1}+\sigma_{11}^0\frac{\partial^2 u}{\partial x_1^2}+\frac{\partial T_{32}}{\partial x_2}+\sigma_{22}^0\frac{\partial^2 u}{\partial x_2^2}$$

$$\rho\frac{\partial^2 u}{\partial t^2}=\frac{\partial}{\partial x_1}\left(c_{44}\frac{\partial u}{\partial x_1}+e_{15}\frac{\partial \phi}{\partial x_1}\right)+\sigma_{11}^0\frac{\partial^2 u}{\partial x_1^2}+\frac{\partial T_{32}}{\partial x_2}+\sigma_{22}^0\frac{\partial}{\partial x_2}\left(T_{32}+\frac{e_{24}}{\varepsilon_{22}}D_2\right)/\Gamma$$

$$\rho\frac{\partial^2 u}{\partial t^2}=(c_{44}+\sigma_{11}^0)\frac{\partial^2 u}{\partial x_1^2}+e_{15}\frac{\partial^2 \phi}{\partial x_1^2}+\left(1+\frac{\sigma_{22}^0}{\Gamma}\right)\frac{\partial T_{32}}{\partial x_2}+\frac{\sigma_{22}^0}{\Gamma}\frac{e_{24}}{\varepsilon_{22}}\frac{\partial D_2}{\partial x_2}$$

$$\Psi\frac{\partial T_{32}}{\partial x_2}=[-\rho\omega^2+k^2(c_{44}+\sigma_{11}^0)-\alpha\, e_{15}k^2]u_3+[e_{15}k^2+\alpha\,\varepsilon_{22}k^2]\phi-\alpha\, q\,\Delta p+\alpha\, q\,\Delta n \quad (27)$$

where $\Gamma=c_{44}+\frac{e_{24}^2}{\varepsilon_{22}}$, $\Psi=\left(1+\frac{\sigma_{22}^0}{\Gamma}\right)$, and $\alpha=\frac{\sigma_{22}^0}{\Gamma}\frac{e_{24}}{\varepsilon_{22}}$

Numerical Results and Discussion

In this section, we present the discussion of the results obtained through computer simulations from the numerical developments in the previous sections for a piezoelectric semiconductor plate (ZnO), whose material parameters and constants are defined as [10] :

$c_{44}=43\ GPa, e_{15}=-0.48\ C/m^2, \varepsilon_{11}=7.61\times10^{-11}F/m, \rho=5700\ kg/m^3$

$n_0=1.2\times10^{23}m^{-3}, \mu^n=130\times10^{-4}m^2/Vs,$

$p_0=2\times10^{24}m^{-3}, \mu^p=34\times10^{-4}m^2/Vs,$ and $D^{n/p}=\mu^{n/p}k_BT/q$

k_B is the Botlzmann constant and T is the absolute temperature. At room temperature $k_BT/q=0.026\ V$. We set the $h=1\ \mu m$ with the total thickness is $2\ \mu m$ as shown in Figure 1.

The numerical computations have been performed with the help of MATLAB software employing the procedure outlined in section 4 for the different modes of SH waves. Here the quantity kh denotes the non-dimensional wave number of acoustic waves traveling in the piezoelectric semiconductor plate.

Approach validation

To check the validity and the efficiency of our approach, a comparison between the obtained results for SH wave and those found in the literature [10]. While Figure 2(a) is the dispersion curves of our results, Figure 2(b) represents those obtained by [10]. It can be seen that our results are in accordance with those of the published data, proving that our approach and program are valid.

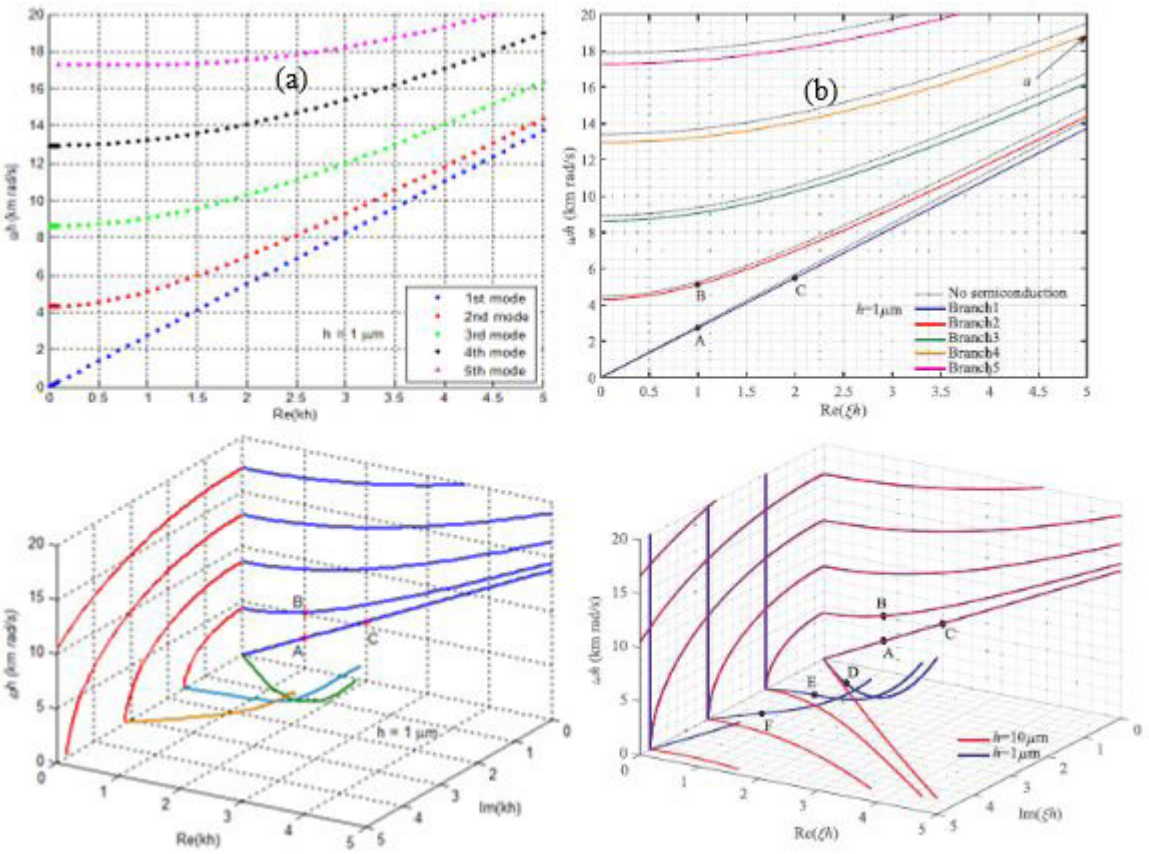

Figure 2: The comparison of dispersion curves: **(a)** results from the present method; and **(b)** results from literature [10]

Effect of initial horizontal stress σ_{11}^0

As previously mentioned in Eq. (1a), the presence of the initial stress σ_{kj}^0 in the piezoelectric semiconductor plate is often inevitable due to chemical shrinkage, material growth, enhancing fracture toughness, mismatching thermal expansion, machining at different temperature values, creep deformation, etc. This initial mechanical stress for the PSC plate ZnO might lead to the dramatic change in the characteristics of the guided waves. Based on the above numerical approach, we calculate the effect of initial stress on the characteristics of SH waves in PSC plate using MATLAB program codes.

Figure 3 shows the dispersion curves of SH waves with and without initial stress, where the left-hand side is for imaginary wavenumber case and the right-hand side is for real wavenumber case. For the curves in Figure 3, there is only one group of dispersion curves, i.e., the one going to the zero frequency as wave number changes from real to pure imaginary. This leads to an energy trapping phenomenon because the real wave number represents a cyclical wave while the imaginary wave number represents a decayed wave.

Here, only one initial horizontal stress component either positive or negative, denoted by σ_{11}^0, exists in the piezoelectric semiconductor plate along the propagating direction. These two applied cases are considered and shown in Figure 3, where the initial stress is tensile of + 0.1 GPa and + 0.5 GPa, and the initial stress is compressive of - 0.1 GPa and - 0.5 GPa are used in the horizontal direction, respectively, In other words, the direction of wave propagation is parallel to the initial stress direction. Here, while the "+" symbol shows a tensile stress, the "-" symbol means compressive one. It is clear at this level that the effects of the initial stress on the dispersion curves are different for the tensile stress case and the compression stress case. The dispersive curves emanating from tensile stress shift to the right side of the dispersive curves with zero stress, while the dispersive curves coming from the compression stresses shift to the left side of the dispersive curves without initial stress in real wave number range, which is reversed in the imaginary wave number range. Meanwhile, it can be observed that despite a slight drift for higher order wavenumber, the dispersion curves of three modes have almost no visible changes for the lowest wavenumber in general.

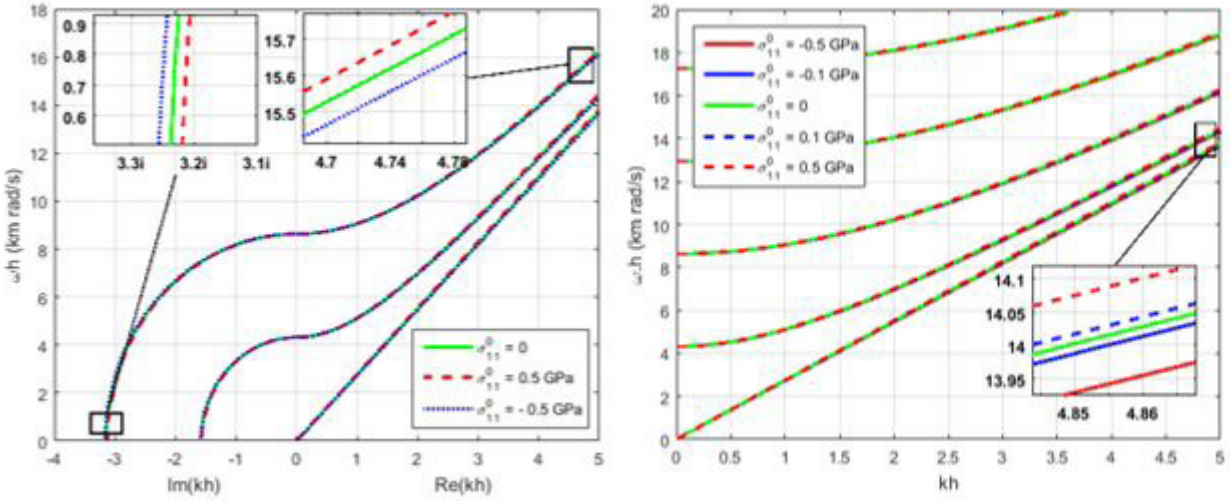

Figure 3: Dispersion curves of SH waves propagating along the polarization direction c-axis x_3 subjected to the initial horizontal stress $\pm\sigma_{11}^0$

More detailed analyses of the investigation of the effect of the initial horizontal stress of the three SH modes are shown in Figure 4. Hence, we used $\Omega = \omega h$ as the dimensionless frequency to plot the relative dimensionless frequency defined as $\Delta\Omega = (\Omega - \Omega^*)/\Omega^*$, it is considered in Figures 4 and 6, in which $\Omega^*$is the frequency of PSC plate without initial stress, Ω belongs to PSC plate with initial stress.

Figure 4 presents a comparison of the product of frequency and thickness changes as a function of kh for the SH_0, SH_1 and SH_2 waves modes at fluctuating initial horizontal tensile and compression stresses. This plot indicates broad changes in relative frequency for higher kh value that reduces in the region of larger kh value at SH_1 and SH_2 modes. Furthermore, the initial stress is given in a certain percentage of the average value of relative frequency and expands up to 0.11% and 0.53%, corresponding to a level of 0.1 and 0.5 GPa, respectively. Hence, it can be seen that the change of relative frequency is linear with the applied initial horizontal stress at fundamental mode SH_0. The ±0.5 GPa in this case (SH0) is roughly ±0.58 % of the greatest tensile and compression strength of the plate.

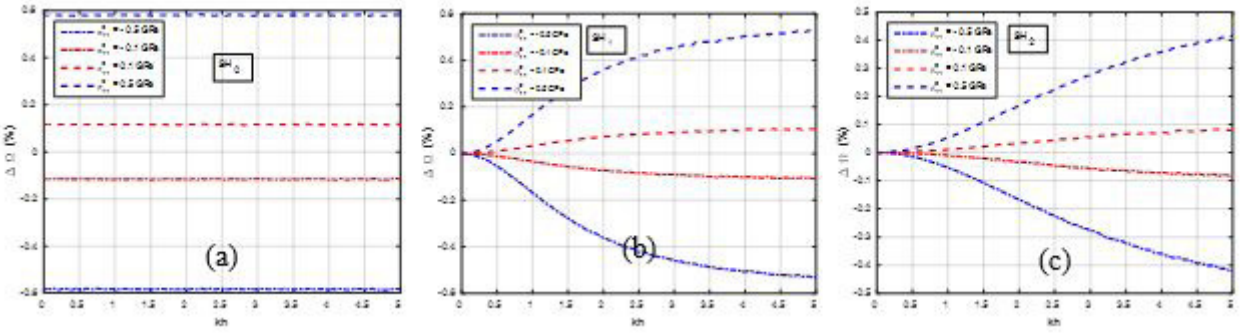

Figure 4: Change in relative frequency versus kh for the SH_0, SH_1 and SH_2 modes with applied initial horizontal stress $\pm\sigma_{11}^0$

Effect of initial vertical stress σ_{22}^0

The present section is continuation of the study of the effect of vertical initial stress. Figure 5 is a plot of dispersion curves of SH waves spreading along the normal direction to the piezoelectric semiconductor plate subjected to the initial vertical stress. The initial stress of ± 0.1 GPa and ± 0.5 GPa are equally employed in the vertical direction, where the "+" symbol implies a vertical tensile stress, and the "-" symbol is a conversely compressive stress. As expected, and as shown in Figure 3, these dispersion curves of phase velocity

appear to be almost indistinguishable to the ones obtained using the initial horizontal stress. The phase velocity changes due to the applied initial vertical stress are still not visible at this scale for the SH modes.

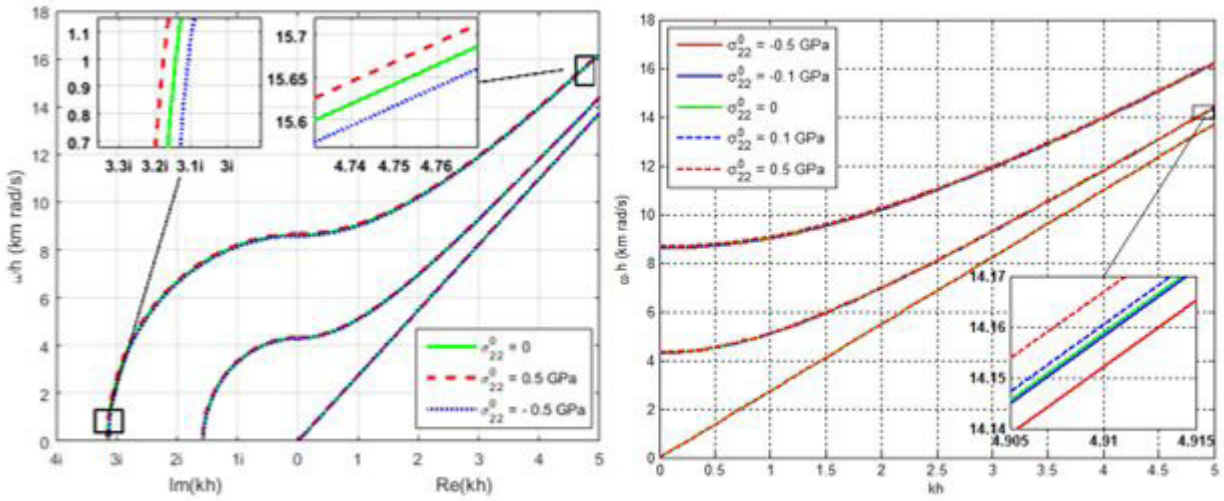

Figure 5: Dispersion curves of SH waves propagating along the polarization direction c-axis x_3 subjected to the vertical initial stresses $\pm\sigma_{22}^0$

Figure 6 further gives the relative frequency changes versus the product of wavenumber and thickness (kh) for the SH wave modes at varying initial vertical stress values. Correspondingly with Figure 4, the dramatic kh changes in relative frequency are seen roughly below the region of kh < 3.5 and the variation approaches to zero in the area of high value. It is clearly noted that the relative frequency is quite large when kh is small, and the variation turns to be much smaller as kh becomes larger. Then the overall magnitude in Figure 6 is similar to those found in Figure 4. Another substantial observation is that SH0 mode is not affected by the loading of initial vertical stress compared to the circumstance of the applied initial horizontal stress in Figure 4a.

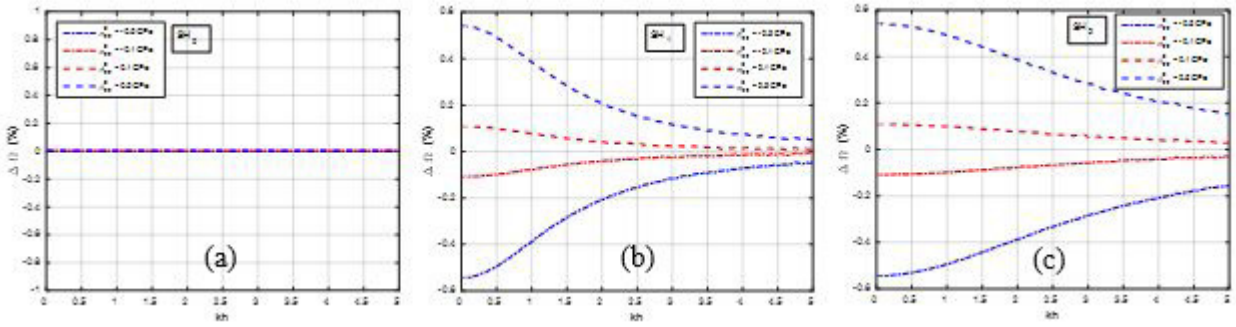

Figure 6: Change in relative frequency versus kh for the SH_0, SH_1 and SH_2 modes with applied initial vertical stress $\pm\sigma_{22}^0$

Wave mode shapes

In this part, modal analysis is performed for SH waves propagating in a piezoelectric semiconductor plate. The through-thickness distributions of some physical quantities are shown in Figure 7 and 8 for the initial horizontal stress and in Figure 9 and 10 for the initial vertical stress on the SH0 and SH1 modes behaviors. The real wavenumber is taken to be $\mathrm{Re(k)} = 1\ \mu m^{-1}$. The values of sampling points are shown in Tables 1 and 2 in detail for the different values of the initial horizontal stress $\sigma_{11}^0 = \pm 0.1\ GPa$ and $\sigma_{11}^0 = \pm 0.5\ GPa$ (Tensile) and initial vertical stress $\sigma_{22}^0 = \pm 0.1\ GPa$ and $\sigma_{22}^0 = \pm 0.5\ GPa$ (Compression). These values are extracted from the results of Figure 3 and 5 for the frequency spectra.

We present 3D figures of the displacement, potential, concentrations of holes and concentrations of electrons, namely Figure 5a,b,c

and d, respectively, when the values on the range of x_1 are all calculated in one wavelength equal to $2\pi/\mathrm{Re(k)}$. Thus, the range is from 0 to 6.28 μm with $\mathrm{Re(k)} = 1\ \mu m^{-1}$. The wave modes in the cycle of $2\pi/\mathrm{Re(k)}$ is enough due to the item $exp(ikx_1)$ in Eq. (24). For the range of x_2, the displacement and concentrations of holes and electrons are calculated along the thickness of the plate ranging from -h to h, i.e. -1 μm to 1 μm. However, the potential is calculated from -2 μm to 2 μm, including the bottom free space from -2 μm to -1 μm, the plate from -1 μm to 1 μm, and the top free space from 1 μm to 2 μm.

Neverthless, to further understand the influence of the initial stress, it is crucial to study the shape of the displacement u_3, potential ϕ and concentrations of holes Δp and electrons Δn (in SH0 and SH1 modes) for $\mathrm{Re(k)} = 1\ \mu m^{-1}$. Figure 7 and 8 illustrate the shapes of u_3, ϕ , Δp, Δn in 3D plot, associated with each distribution $x_1 = 0$ and $x_1 = 1.5\ \mu m$ for SH0 and SH1 mode, respectively. It can be seen from Figure 7 and 8 that the holes concentration Δp has the same distribution as the displacement u_3, while the electron concentration Δp has a converse distribution. A similar tendency can also be seen for the potential ϕ. The point where $Re(k)$ equals 1 μm^{-1} has a very small $Im(k)$ compared to $Re(k)$ as shown in Tables 1 and 2. Comparing the point when $Re(kh) = 1$ of modes SH0 and SH1, the typical wave mode shapes for SH waves reveal that SH0 is the lowest mode. Besides, while for the latter, the u_3, ϕ , Δp, Δn are all constant across the plate, for the SH1 mode, they all have nodes

Initial horizontal stress		Frequency ω $(\times\ 10^9\ \mathbf{rad/s})$	$\mathbf{Im}\ (k)\ (\times 10^{-6}\mu m^{-1})$
$\sigma_{11}^0 = 0$	SH_0	2.746609497585986	5.507886600276184
	SH_1	**5.114453576696010**	**35.63463632820050**
$\sigma_{11}^0 = 0.1\ GPa$	SH_0	2.749801374043001	5.507886600276184
	SH_1	**5.116168611671140**	**36.12212002144940**
$\sigma_{11}^0 = 0.5\ GPa$	SH_0	2.762532040240010	5.80080902200120
	SH_1	**5.123022295966911**	**34.92212028636439**
$\sigma_{11}^0 = -0.1\ GPa$	SH_0	2.743413907221299	5.506001022752010
	SH_1	**5.112738225147944**	**37.06212019601206**
$\sigma_{11}^0 = -0.5\ GPa$	SH_0	2.730594148906415	5.502830120186227
	SH_1	**5.105870527149874**	**37.07229011482149**

Table 1: Values of imaginary wavenumbers and frequencies for different values of initial horizontal stress with $Re(k) = 1\ \mu m^{-1}$

Initial vertical stress		Frequency ω $(\times\ 10^9\ \mathbf{rad/s})$	$\mathbf{Im}\ (k)\ (\times 10^{-6}\mu m^{-1})$
$\sigma_{22}^0 = 0$	SH_0	2.74660949750	5.50788660027
	SH_1	**5.11445357669**	**35.6346363282**
$\sigma_{22}^0 = 0.1\ GPa$	SH_0	2.74660950050	5.52892755279
	SH_1	**5.11840570010**	**35.1478912301**
$\sigma_{22}^0 = 0.5\ GPa$	SH_0	2.74660949050	5.44996600276
	SH_1	**5.13418310012**	**30.6661513995**
$\sigma_{22}^0 = -0.1\ GPa$	SH_0	2.74660947200	5.31860090010
	SH_1	**5.11049719020**	**25.9666151399**
$\sigma_{22}^0 = -0.5\ GPa$	SH_0	2.74660955940	5.97100101201
	SH_1	**5.09464784011**	**49.9666151399**

Table 2: Values of imaginary wavenumbers and frequencies for different values of initial vertical stress with $Re(k) = 1\ \mu m^{-1}$

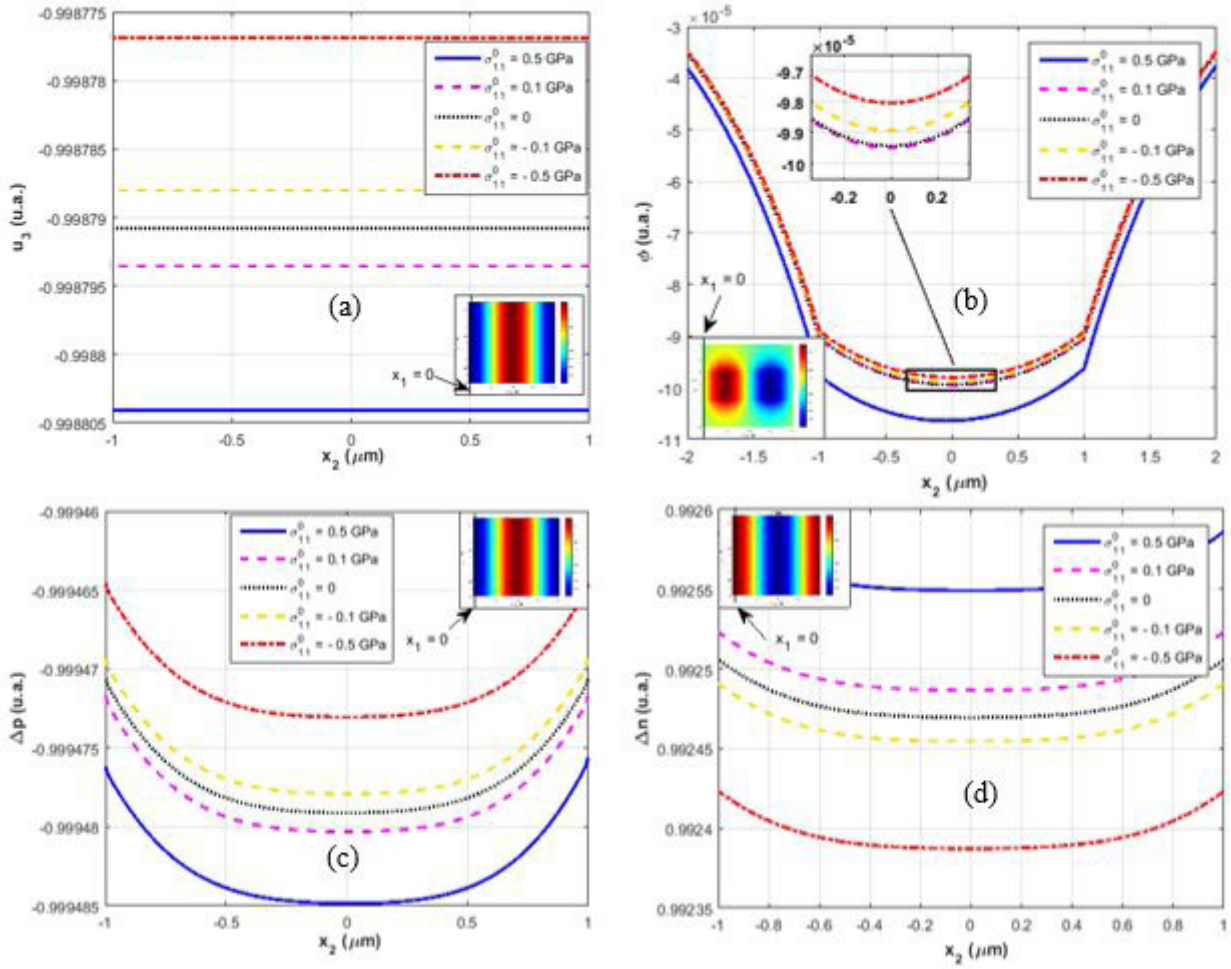

Figure 7: Effects of initial horizontal tensile and compressive stress on electromechanical fields **(a)** Displacement, **(b)** Electric potential, **(c)** concentration of holes, **(d)** concentration of electrons for SH0 mode at $kh = 1$

Figures 8b and 10breveal that when an initial horizontal stress was applied, positive piezoelectric polarization charges appeared at the top surface while negative charges appeared at the bottom surface (caused by the piezoelectric effect of PSC). This resulted in the decrease of the concentration of holes at the top boundary layer and the increase of the concentration at the bottom surface, as shown in Figures 8c and 10c.

Therefore, it is obviously seen from Figures 7a and 9a that the horizontal initial stress increases from -5 GPa to 0.5 GPa. Furthermore, the variation of the displacement u_3 for SH0 mode increases linearly, but in the case of the applied vertical initial stress, it shows the opposite phenomenon. Thus, the effect of vertical initial stress is also observed to be more significant than that of the horizontal initial stress applied in PSC plate for the SH0 mode represented in Figures 7b and 9b.

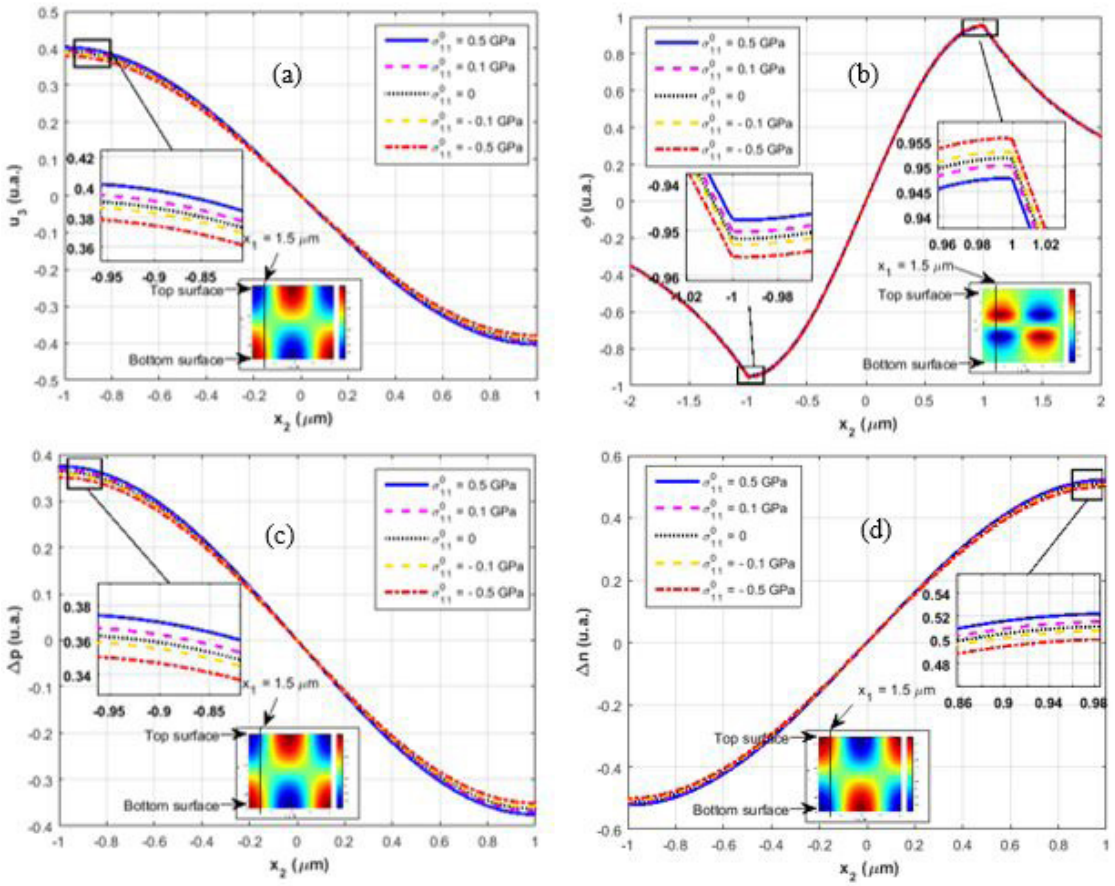

Figure 8: Effects of initial horizontal tensile and compressive stress on electromechanical fields **(a)** Displacement, **(b)** Electric potential, **(c)** concentration of holes, **(d)** concentration of electrons for SH1 mode at $kh = 1$

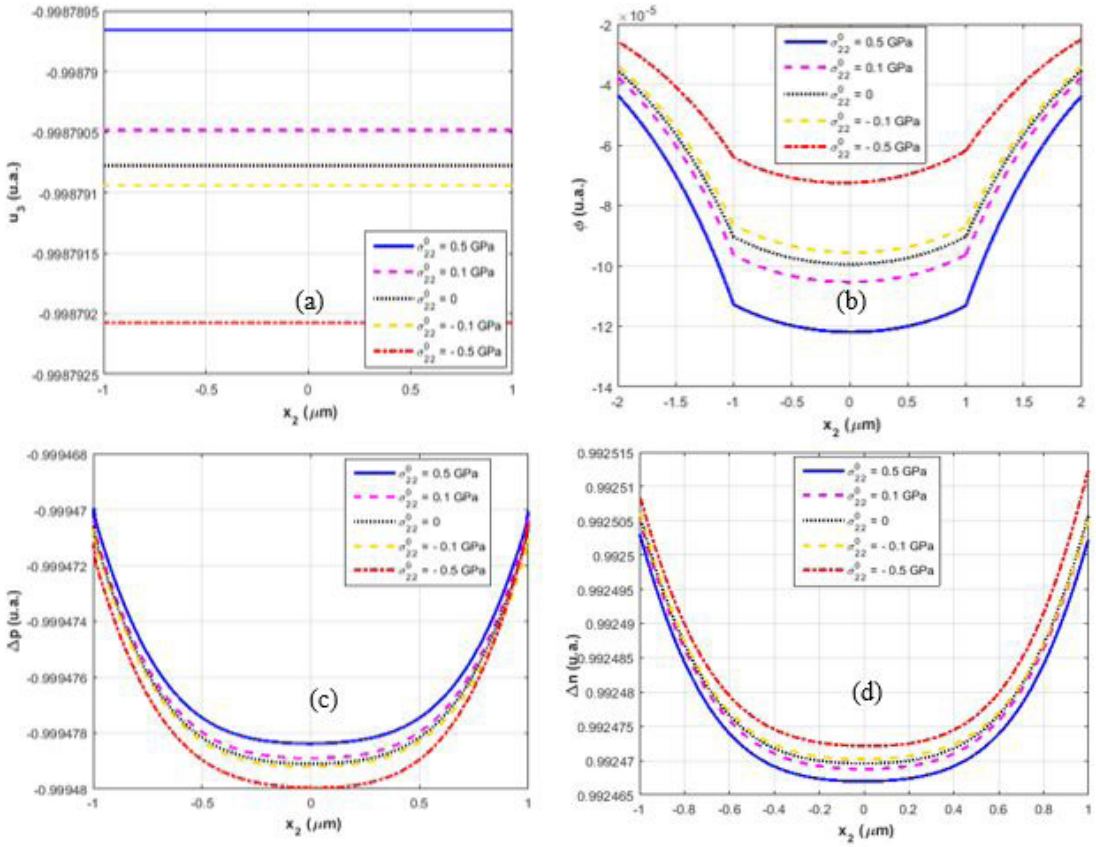

Figure 9: Effects of initial vertical tensile and compressive stress on electromechanical fields **(a)** Displacement, **(b)** Electric potential, **(c)** concentration of holes, **(d)** concentration of electrons along the PSC ZnO plate for SH0 mode at $kh = 1$

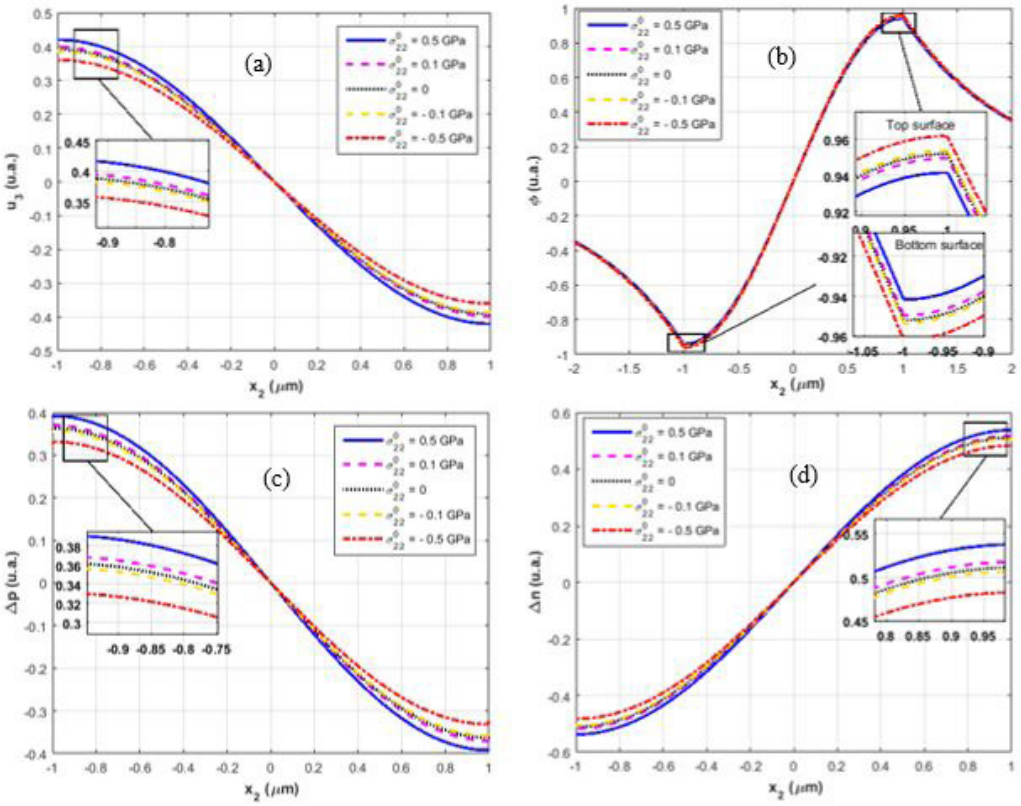

Figure 10: Effects of initial vertical tensile and compressive stress on electromechanical fields **(a)** Displacement, **(b)** Electric potential, **(c)** concentration of holes, **(d)** concentration of electrons along the PSC ZnO plate for SH1 mode at $kh = 1$

Conclusions

In the present research work, the propagation of SH-type wave under an initial horizontal and vertical stress of a piezoelectric semiconductor plate was numerically investigated. The phase velocity of SH0, SH1 and SH2 modes waves were calculated for various initial stress σ_{ij}^0 values. The initial horizontal stress was proven to have a significant influence on SH wave behaviors, especially in high wavenumber. It was found that the existence of an initial vertical stress led to the increase in the phase velocity on the range of low wavenumber. From the calculated phase velocity spectra, it was demonstrated that the tensile initial stress would increase the phase velocity of SH waves propagating in the PSC plate, while the compressive initial stress would reduce the phase velocity.

The components of displacement, potential, hole concentration and concentration electrons of SH wave were obtained using a numerical treatment. In fact, the initial horizontal and vertical stresses acting in the plate PSC were confirmed to have a considerable influence on the component of displacement of mode SH0 compared to mode SH1. However, the initial stresses acting in the PSC plate remarkably affected only the top and bottom surfaces of PSC plate on the electromechanical fields of the SH1 mode. Furthermore, it is also established that the initial horizontal and vertical stresses have an opposite effect on the components of displacement, hole concentration and concentration electrons of SH0 mode. These numerical results for the piezoelectric semiconductor plate are significant for the improvement of the piezoelectric nanogenerators devices and the design of ultrasonic transducers in industry for non-destructive testing especially that encounters initial stresses.

Highlights

- The propagation of the SAW in the piezoelectric nanogenerators is researched by using numerical matrix method approach.
- The phase velocity of SH0, SH1 and SH2 modes waves are calculated for various initial stress values.
- The obtained results reveal the tensile initial stress will increase the phase velocity (increase the kinetic energy of waves) of SH waves propagating in the PSC plate, while the compressive initial stress will reduce the phase velocity.

- The initial horizontal and vertical stresses acting in the plate PSC have a considerable influence on the component of displacement, potential, hole concentration and concentration electrons of mode SH0 compared to mode SH1.

References

1. Hickernell S (2005) The piezoelectric semiconductor and acoustoelectronic device development in the sixties, IEEE Trans Ultrason Ferroelectr Freq Control 52: 737-45.

2. Hutson AR, White DL (1962) Elastic wave propagation in piezoelectric semiconductors. J Appl Phys 33: 40-7.

3. Zhang Y, Yang Y, Wang ZL (2012) Piezo-phototronics effect on nano/microwire solar cells. Energy Environ Sci 5: 6850-6.

4. Ingebrigtsen KA (1970) Linear and nonlinear attenuation of acoustic surface waves in a piezoelectric coated with a semiconducting film. J Appl Phys 41: 454-9.

5. YH, Wanli Yang JY (2018) Transient Extensional Vibration in a ZnO Piezoelectric Semiconductor Nanofiber Under a Suddenly Applied End Force. Mater Res Express 2018: 1-13.

6. Zhang C, Wang X, Chen W, Yang J (2016) An analysis of the extension of a ZnO piezoelectric semiconductor nanofiber under an axial force. Smart Mater Struct 26: 10.1016/j.snb.2007.07.003.

7. Wang ZL (2003) Nanobelts, nanowires, and nanodiskettes of semiconducting oxides - From materials to nanodevices. Adv Mater 15: 432-6.

8. Wen X, Wu W, Ding Y, Wang ZL (2013) Piezotronic effect in flexible thin-film based devices. Adv Mater 25: 3371-9.

9. Lee KY, Kumar B, Seo JS, Kim KH, Sohn JI, et al. (2012) P-type polymer-hybridized high-performance piezoelectric nanogenerators. Nano Lett 12: 1959-64.

10. Zhu F, Ji S, Zhu J, Qian Z, Yang J (2018) Study on the influence of semiconductive property for the improvement of nanogenerator by wave mode approach. Nano Energy 52: 474–84.

11. Soomro MY, Hussain I, Bano N, Nur O, Willander M (2012) Piezoelectric power generation from zinc oxide nanowires grown on paper substrate. Phys Status Solidi - Rapid Res Lett 6: 80-2.

12. Minne SC, Manalis SR, Quate CF (1995) Parallel atomic force microscopy using cantilevers with integrated piezoresistive sensors and integrated piezoelectric actuators. Appl Phys Lett 67: 3918.

13. Soomro MY, Hussain I, Bano N, Hussain S, Nur O, et al. (2012) Enhancement of zinc interstitials in ZnO nanotubes grown on glass substrate by the hydrothermal method. Appl Phys A Mater Sci Process 106: 151-6.

14. Fei P, Yeh PH, Zhou J, Xu S, Gao Y, et al. (2009) Wang, Piezoelectric potential gated field-effect transistor based on a free-standing ZnO wire. Nano Lett 9: 3435-9.

15. He JH, Hsin CL, Liu J, Chen LJ, Wang ZL (2007) Piezoelectric gated diode of a single ZnO nanowire. Adv Mater 19: 781-4.

16. Zhou J, Fei P, Gao Y, Gu Y, Liu J, et al. (2008) Mechanical-electrical triggers and sensors using piezoelectric micowires/nanowires. Nano Lett 8: 2725-30.

17. Auld BA (1973) Accoustic Fields and Waves in Solids, John Wiley, New York, USA.

18. Pierret RF (1988) Semiconductor Fundamentals, Addison-We, Massachusetts, USA.

19. Li P, Jin F, Yang J (2015) Effects of semiconduction on electromechanical energy conversion in piezoelectrics. Smart Mater Struct 24: 25021.

20. Gu C, Jin F (2015) Shear-horizontal surface waves in a half-space of piezoelectric semiconductors. Philos Mag Lett 95: 92-100.

21. Cao X, Hu S, Liu J, Shi J (2019) Generalized Rayleigh surface waves in a piezoelectric semiconductor half space. Meccanica 54: 271-81.

22. Yang JS, Song YC, Soh AK (2006) Analysis of a circular piezoelectric semiconductor embedded in a piezoelectric semiconductor substrate. Arch Appl Mech 76: 381-90.

23. Zhao MH, Pan YB, Fan CY, Xu GT (2016) Extended displacement discontinuity method for analysis of cracks in 2D piezoelectric semiconductors. Int J Solids Struct 94–95: 50-9.

24. Hu Y, Zeng Y, Yang J (2007) A mode III crack in a piezoelectric semiconductor of crystals with 6 mm symmetry. Int J Solids Struct 44: 3928-38.

25. Zhang CL, Luo YX, Cheng RR, Wang XY (2017) Electromechanical Fields in Piezoelectric Semiconductor Nanofibers under an Axial Force. MRS Adv 2: 3421-6.

26. Fan S, Liang Y, Xie J, Hu Y (2017) Exact solutions to the electromechanical quantities inside a statically-bent circular ZnO nanowire by taking into account both the piezoelectric property and the semiconducting performance: Part I—Linearized analysis. Nano Energy 40: 82-7.

27. Luo Y, Zhang C, Chen W, Yang J (2017) An analysis of PN junctions in piezoelectric semiconductors. J Appl Phys 122: 10.1063/1.4996754.

28. Zhou YY, Lü CF, Chen WQ (2012) Bulk wave propagation in layered piezomagnetic/piezoelectric plates with initial stresses or interface imperfections. Compos Struct 94: 2736-45.

29. Son MS, Kang YJ (2011) The effect of initial stress on the propagation behavior of SH waves in piezoelectric coupled plates. Ultrasonics 51: 489-95.

30. Qian Z, Jin F, Kishimoto K, Wang Z (112) Effect of initial stress on the propagation behavior of SH-waves in multilayered piezoelectric composite structures. Sensors Actuators A Phys 112: 368-75.

31. Qian ZH, Jin F, Lu T, Kishimoto K, Hirose S (2010) Effect of initial stress on Love waves in a piezoelectric structure carrying a functionally graded material layer. Ultrasonics 50: 84-90.

32. Qian ZH, Jin F, Lu TJ, Kishimoto K (2009) Transverse surface waves in a 6 mm piezoelectric material carrying a prestressed metal layer of finite thickness. Appl Phys Lett 94: 10.1063/1.3095922.

33. Guo X, Wei P (2014) Effects of initial stress on the reflection and transmission waves at the interface between two piezoelectric half spaces. Int J Solids Struct 51: 3735-51.

34. Othmani C, Zhang H, Lü C (2019) Effects of initial stresses on guided wave propagation in multilayered PZT-4/PZT-5A composites: A polynomial expansion approach. Appl Math Model 78: 148-68.

35. Othmani C, Zhang H, Lü C, Takali F (2019) Effects of initial stresses on the electromechanical coupling coefficient of SH wave propagation in multilayered PZT-5H structures. Eur Phys J Plus 134: 10.1140/epjp/i2019-12891-7.

36. Othmani C, Labiadh L, Lü C, Kamali AR, Takali F (2020) Influence of a piezoelectric ZnO intermediate layer on Rayleigh waves propagating in Sc43%AlN57%/ZnO/diamond hetero-structures subjected to uniaxial stress. Eur Phys J Plus 135: 10.1140/epjp/s13360-020-00912-9.

37. Shams M (2016) Effect of initial stress on Love wave propagation at the boundary between a layer and a half-space, Wave Motion 65: 92-104.

38. Singhal A, Sahu SA, Chaudhary S (2018) Approximation of surface wave frequency in piezo-composite structure. Compos Part B Eng 144: 19-28.

39. Huang H, Qian Z, Yang J (2019) I-V characteristics of a piezoelectric semiconductor nanofiber under local tensile/compressive stress. J Appl Phys 126: 10.1063/1.5110876.

40. Liu Y, Zhang Y, Yang Q, Niu S, Wang ZL (2014) Fundamental theories of piezotronics and piezo-phototronics. Nano Energy 14: 257-75.

41. Zhang Y, Leng Y, Willatzen M, Huang B (2018) Theory of piezotronics and piezo-phototronics. MRS Bull 43: 928-35.

42. Gao Y, Wang ZL (2007) Electrostatic potential in a bent piezoelectric nanowire. The fundamental theory of nanogenerator and nanopiezotronics. Nano Lett 7: 2499-505.

43. Dai Z, Zhu F, Qian Z, Yang J (2018) Electric potential and carrier distribution in a piezoelectric semiconductor nanowire in time-harmonic bending vibration. Nano Energy 43: 22-8.

44. Jie L, Zhou J (2011) Propagation of Lamb waves in a pre-stressed plate. Appl Mech Mater 66–68: 413-8.